Volume 11 | Number 21 | 7 November 2024

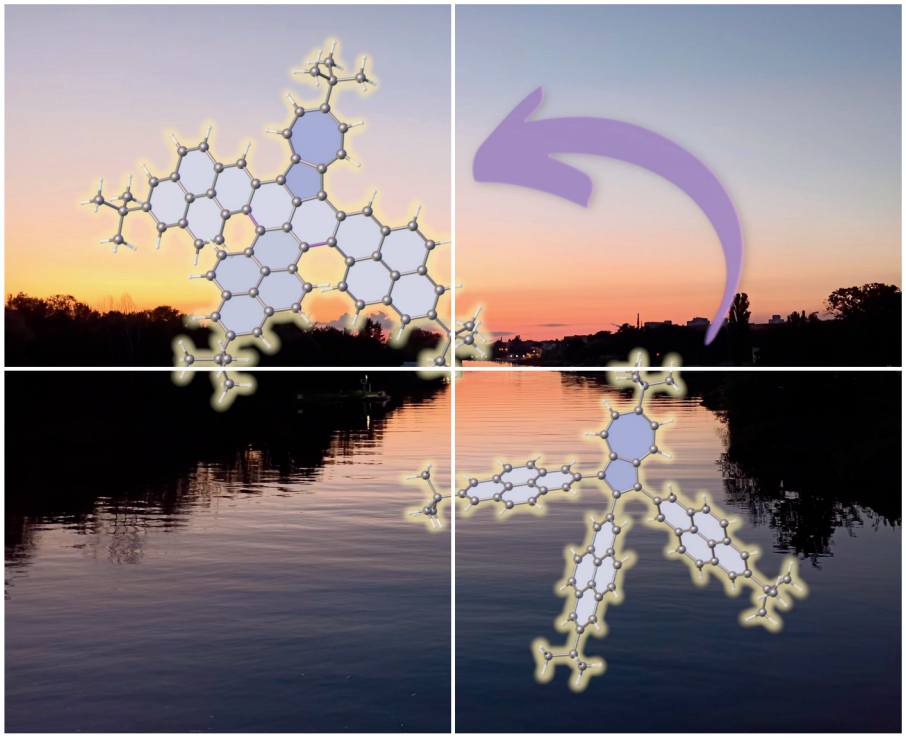

ORGANIC CHEMISTRY

FRONTIERS

CCS 中国化学会 CHINESE CHEMICAL SOCIETY

SIOC 1950

ROYAL SOCIETY OF CHEMISTRY

rsc.li/frontiers-organic

ORGANIC CHEMISTRY FRONTIERS

RESEARCH ARTICLE

View Article Online
View Journal | View Issue

Cite this: *Org. Chem. Front.*, 2024, **11**, 6026

1,2,3-Triarylazulenes as precursors of azulene-embedded polycyclic aromatic hydrocarbons†‡

Justyna Biesaga, Sławomir Szafert and Bartłomiej Pigulski *

A series of 1,2,3-triarylazulenes was obtained using new synthetic methodology and subsequently subjected to Scholl-type oxidation aiming for conjugated azulene-embedded polycyclic aromatic hydrocarbons (PAHs). The oxidation yielded either unexpected azulen-1(8a*H*)-ones or desired purely hydrocarbon azulene-embedded PAHs, depending on the substitution pattern. Different reaction pathways were rationalized using DFT calculations, leading to the observation that 2-pyrenyl substituents facilitate formation of the desired conjugated molecules. The fully hydrocarbon azulene-embedded PAHs exhibit a relatively small electrochemical energy gap below 2 eV and optical absorption reaching the near-infrared (NIR) region. These properties are attributed to their non-alternant topology and retained azulene-like electronic structure.

Received 7th August 2024,
Accepted 11th September 2024

DOI: 10.1039/d4qo01459f

rsc.li/frontiers-organic

Introduction

The discovery of fullerenes, carbon nanotubes, and graphene has initiated extensive research into new carbon allotropes and carbon-rich molecules.[1] A diverse array of benzenoid polycyclic aromatic hydrocarbons (PAHs), or in other words, nanographenes, has been synthesized using a bottom-up approach.[2,3] There is also a growing interest in the chemistry of non-alternant π-scaffolds containing five- or seven-membered rings due to their distinctive properties compared to fully benzenoid PAHs.[4–6]

Azulene, in particular, is a highly sought-after non-alternant structural motif in PAHs due to its unique electronic properties, including a small highest occupied molecular orbital-lowest unoccupied molecular orbital (HOMO–LUMO) gap or emission from the S_2 state, which disobeys Kasha's rule.[7,8] These properties stem from azulene's electronic structure, which effectively functions as a fused tropylium ion and cyclopentadienyl anion with an inherent dipole moment 1.08 D and significant spatial separation between the HOMO and LUMO orbitals (Scheme 1a).[9] PAHs containing azulene structural motifs exhibit unique properties such as warped structure,[10] biradical characteristics,[11,12] and near-infrared (NIR) absorption,[13] which make them suitable for applications in organic electronics,[14,15] solar cells,[16–20] bioimaging,[21] and single-molecule devices.[22]

Faculty of Chemistry, University of Wrocław, 14 F. Joliot-Curie, 50-383 Wrocław, Poland. E-mail: bartlomej.pigulski@uwr.edu.pl

† Dedicated to Prof. Frank Würthner on the occasion of his 60th birthday.

‡ Electronic supplementary information (ESI) available: Experimental procedures, details of X-ray single crystal diffraction experiments, copies of UV/Vis/NIR spectra, copies of NMR spectra, copies of electrochemical measurements, and Cartesian coordinates of DFT-optimized structures. CCDC 2371233–2371235. For ESI and crystallographic data in CIF or other electronic format see DOI: https://doi.org/10.1039/d4qo01459f

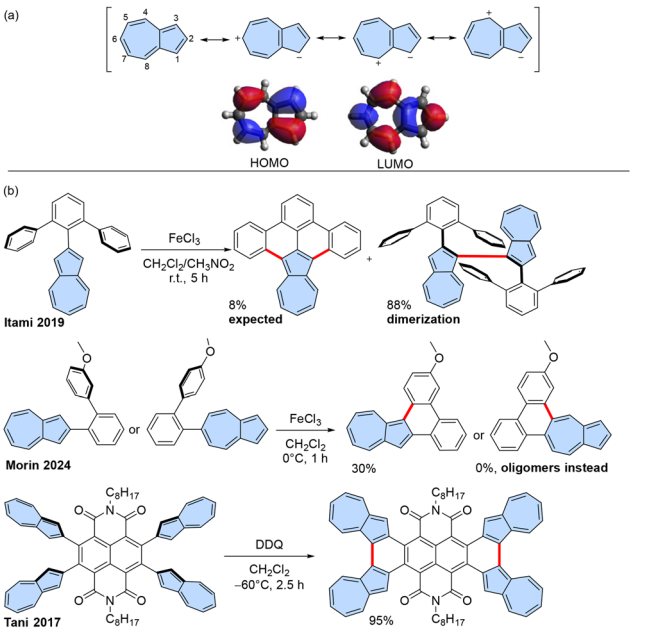

Scheme 1 (a) Azulene: selected resonance structures, molecular frontier orbitals, and position numbering. (b) Synthesis of conjugated azulene-embedded PAHs using Scholl-type oxidation.

The rapid development of synthetic methods for functionalized azulenes[23–25] and azulene-embedded PAHs[4,26] can be attributed to the diverse and intriguing properties of these compounds. In some cases, azulene or a 'formal azulene' moiety is formed in the last step of the synthetic pathway. However, the key step often involves the fusion of precursors that already contain azulene subunits, finally resulting in a fully conjugated π-system. Various chemical transformations have been employed to achieve conjugated π-systems, such as the annulation of alkenes[27] or annulation of alkynes.[28,29] Additionally, more complex approaches such as tandem Suzuki coupling followed by condensation might be realized in two steps[30,31] or in one step.[32]

Several additional strategies have been developed for the synthesis of azulene-embedded PAHs, including palladium-catalysed Heck-type intramolecular cyclization,[33] [3 + 3] palladium-catalysed tandem Suzuki coupling and C–H arylation,[13] or cyclization of substituted 1-nitroazulenes.[34] However, there are limitations to all these methods, and therefore, the need remains for more efficient synthetic methodologies for azulene-embedded PAHs.

Scholl oxidation is a very potent synthetic tool leading to various PAHs, but in many cases, the exact reactivity pattern is not easy to predict.[35,36] Consequently, Scholl-type oxidation and related Mallory photo-oxidation have been employed for some azulene-embedded PAHs (Scheme 1b), although these reactions often yield suboptimal results in terms of yield and selectivity.

Because positions 1 and 3 of the azulene moiety are the most electron-rich, precursors of azulene-embedded PAHs are typically targeted for oxidation in the synthesis of azulene-embedded PAHs. However, the tendency of azulene to form 1,3-polyazulene upon oxidation[37] might result in dimerization of azulene rather than the desired fused molecule. For instance, Itami and co-workers[38] reported that the expected fully fused product was isolated only in 8% yield after oxidation with $FeCl_3$, while the main product of 1,1′-biazulene was obtained in 88% yield. Recently, Morin and co-workers reported attempts to achieve fused products.[39] However, the reaction yield was low (30%) when position 1 of azulene was involved in oxidation, and attempts to fuse position 5 resulted exclusively in oligomeric products.

Intramolecular fusion of azulene units is more efficient when performed in an electron-deficient system, as demonstrated by Tani and co-workers[40] in their synthesis of azulene-fused tetracene diimide. Mallory photo-oxidation has also proven useful, as shown by Zhang and coworkers.[41] All examples of known syntheses of azulene-embedded PAHs involve oxidation positions 1 and 3 of azulene, where the HOMO is primarily located, and which are the most electron-rich positions. However, having such positions unsubstituted can lead to competitive intermolecular oxidation and a lower yield of the desired intramolecular product, such as in the example reported by Itami.[38]

Herein, we report the synthesis of a series of 1,2,3-triarylazulenes, and the application of these triarylazulenes in Scholl-type reactions for the first time. Interestingly, depending on the substitution pattern, oxidation leads either to a 1,2-shift of a phenyl group or to partially and fully fused products.

Results and discussion

Synthesis of precursors

The primary rationale for using 1,2,3-triarylazulenes as precursors for fused azulene-embedded PAHs was the fact that the highly reactive positions 1 and 3 are pre-blocked before the oxidation step. It is expected that this approach will prevent the formation of oligomeric products and lead to the desired fully-fused azulene-embedded PAHs.

Despite interesting photophysical properties,[42] known examples of 1,2,3-triarylazulenes are quite limited. Existing syntheses typically start from substituted tolanes where the crucial step involves expansion of a phenyl ring, which significantly reduces the available substitution patterns. These reactions are usually catalysed using sulfenyl chloride/$AlCl_3$,[43,44] palladium catalyst,[45] or gold catalyst.[46]

Hence, we developed a novel modular approach for 1,2,3-triarylazulenes (Scheme 2) that enables selective placement of substituents at positions 1, 2, and 3. We utilized two types of selective reactions: borylation (position 2) and iodination (positions 1 and 3). The synthesis began with the known 6-*tert*-butylazulene,[47] which was selected for its increased solubility compared to unsubstituted azulene. Subsequently, 6-*tert*-butylazulene underwent borylation at position 2 *via* modified iridium(I)-catalysed C–H borylation,[48] giving compound **5** in 66% isolated yield. Azulen-2-ylboronic acid pinacol ester **5** was later subjected to the Suzuki coupling with haloarenes. The lower yield of compound **6b** was likely due to its poor solubility, which resulted in difficulties during its isolation. All compounds **6a–6c** underwent double iodination using *N*-iodosuccinimide (NIS), yielding compounds **7a–7c** in high yields from 84% to 98%.

The final step in the synthesis of 1,2,3-triarylazulenes was the double Suzuki coupling with boronic acids (4-anisyl and 4-*tert*-butylphenyl substituents) or boronic acid pinacol ester (2-(7-*tert*-butylpyrenyl) substituent). The final coupling reactions were catalysed using $Pd(dppf)Cl_2{\cdot}CH_2Cl_2$, and the products were isolated in decent yields from 46% to 92%. Finally, a set of 1,2,3-triarylazulenes **1a–1f** was synthesized using this modular approach and subsequently employed in Scholl-type oxidation.

Scholl-type oxidation

With a series of 1,2,3-arylazulenes available, we aimed to optimize the oxidation conditions to achieve fully fused products. Precursor **1a** was selected as a convenient model substrate for the Scholl reaction, and various conditions were tested, aiming for fully fused product **2a** (Table 1). Initially, we used 2,3-dichloro-5,6-dicyano-1,4-benzoquinone (DDQ) as an oxidant (entries 1 and 2). However, in the presence of MsOH, the sub-

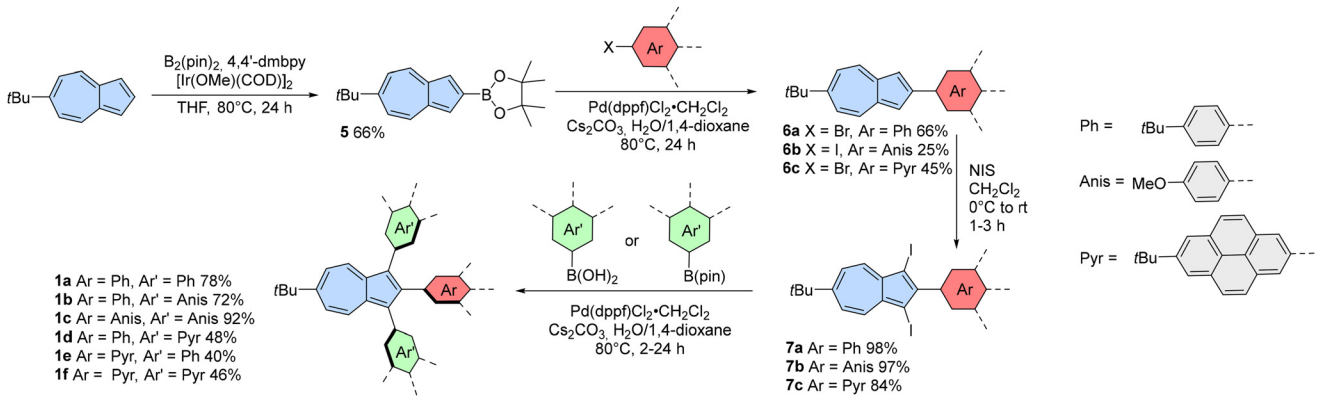

Scheme 2 Synthesis of azulene-containing precursors **1**. $B_2(pin)_2$ = bis(pinacolato)diboron, 4,4′-dmbpy = 4,4′-dimethyl-2,2-dipyridyl, COD = 1,5-cyclooctadiene, THF = tetrahydrofuran, dppf = 1,1′-bis(diphenylphosphino)ferrocene, NIS = *N*-iodosuccinimide.

Table 1 Optimization of the Scholl-type reaction for precursor **1a**

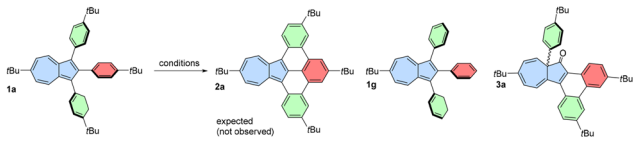

	Oxidant	Conditions	Result
1	DDQ, MsOH	CH_2Cl_2, 0 °C, 24 h	**1a** recovered
2	DDQ	CH_2Cl_2, rt, 17 h	Decomposition
3	$AlCl_3$	PhCl, 80 °C, 48 h	**1g** (quant.)
4	$MoCl_5$	CH_2Cl_2, rt, 17 h	Decomposition
5	$FeCl_3$	CH_2Cl_2/$MeNO_2$, −78 °C to 0 °C, 20 h	**1a** recovered
6	$FeCl_3$	CH_2Cl_2/$MeNO_2$, rt, 20 h	Decomposition
7	**$FeCl_3$, K_2CO_3**	**DCE/$MeNO_2$, 80 °C, 19 h**	**3a** (93%)[a]

[a] Yields after isolation.

strate was recovered after the reaction, while in the absence of acid, the reaction resulted only in the decomposition of the starting material.

This fact suggested that the protonated form of azulene might be not oxidized under these conditions. Surprisingly, the reaction using $AlCl_3$ in chlorobenzene (entry 3) led to almost quantitative removal of *tert*-butyl groups from phenyl rings and formation of **1g**. Oxidation using $MoCl_5$ led only to an unidentified mixture of products (entry 4), but after oxidation using $FeCl_3$ at low temperature (entry 5), we recovered only the starting material. Additionally, when oxidation was conducted at room temperature, then only decomposition of the substrate was observed (entry 6).

We noted that the reaction mixture turned from green to very intense red after addition of $FeCl_3$/$MeNO_2$ to the solution of starting azulene. This suggested that in the presence of residual moisture, azulene can be protonated, and this hinders the desired reaction. Based on this observation, we hypothesized that adding a base to the reaction system could drive the reaction in the desired direction. Indeed, the addition of K_2CO_3 and switching to 1,2-dichloroethane (DCE) from CH_2Cl_2 along with a higher reaction temperature led to the product that was initially believed to be oxidized **1a** with one new C–C bond formed (entry 7). However, the ^{13}C NMR spectrum of the pale yellow product revealed a typical carbonyl signal above 200 ppm, indicating that azulen-1(8a*H*)-one **3a** was the actual product of oxidation. This unprecedented oxidation involves a 1,2-aryl shift, oxidation of the most electron-rich position of azulene, and formation of a new C–C bond between adjacent phenyl groups.

We extended our investigation to the oxidation of a broader range of 1,2,3-triarylazulenes under designed conditions (Scheme 3). Precursor **1b** gave similar pale-yellow azulen-1(8a*H*)-one **3b** in 58% yield after extending the reaction time to 96 h. Substrate **1c** bearing three methoxy groups also gave the product of 1,2 phenyl shift **3c**, but no formation of C–C bond was observed even after two days. Additionally, a more prolonged reaction time led only to a gradual decomposition of **3c**. To the best of our knowledge, this represents the first oxidation and 1,2 phenyl shift leading from azulene to azulen-1(8a*H*)-one. Previously, azulen-1(8a*H*)-ones have been synthesized through rhodium-[49] or gold-catalysed[50] cyclizations of diazo compounds or cycloadditions involving ketenes and alkynes.[51,52]

We also attempted to verify the origin of the oxygen atom in products **3a–3c**. It is highly unlikely that residual O_2 was involved, as the reaction mixture was carefully degassed. We hypothesized that the oxygen might originate from residual moisture in K_2CO_3 and/or $FeCl_3$, or possibly from the decomposition of K_2CO_3. To test this hypothesis, we conducted oxidation reactions of **1a** and **1b** with the addition of isotopically labelled H_2O (97% ^{18}O). Unfortunately, the added water quenched the reaction, which prevented us from drawing any definitive conclusions.

The formation of azulen-1(8a*H*)-ones was an intriguing observation, but it was not the initial goal of using 1,2,3-triarylazulenes as substrates in the Scholl oxidation. Inspired by literature precedents,[53] we aimed to use azulenes **1d–1f** bearing one, two, or three phenyl substituents replaced with 2-pyrenyl substituents to obtain fully fused azulene-embedded PAHs.

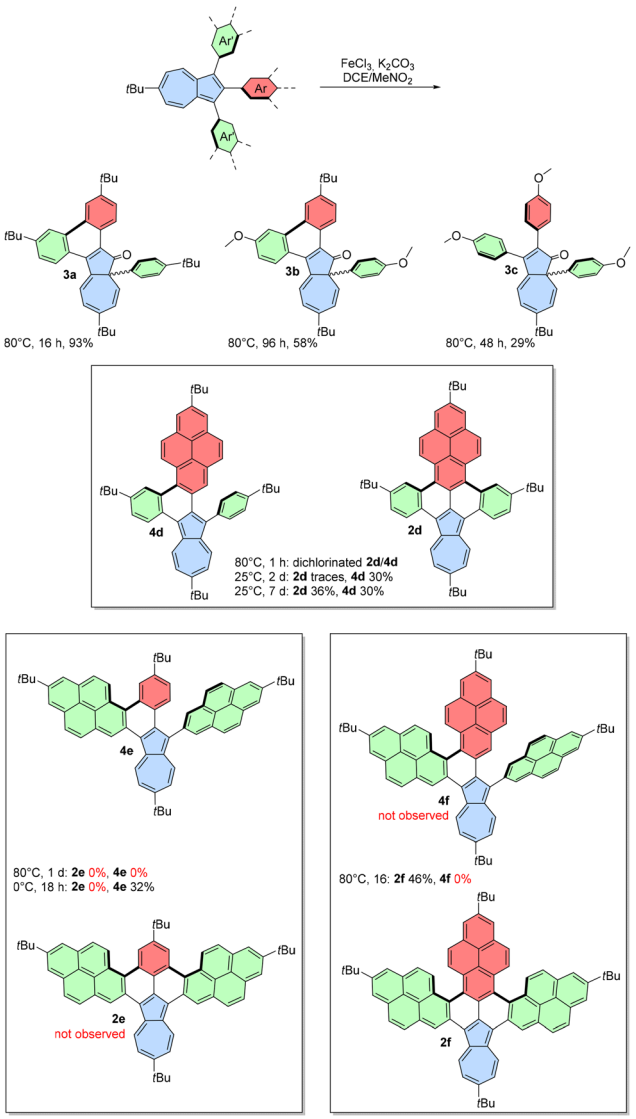

Scheme 3 Scholl-type oxidation of azulenes **1a–1f** (yields after isolation).

Indeed, incorporating one or more 2-pyrenyl substituents shifted the reactivity pattern in the desired direction. The oxidation of **1d** was initially carried out at 80 °C, which unfortunately led to significant decomposition and an undesired side reaction, as evidenced by atmospheric-pressure chemical ionization (APCI) mass spectra showing a mixture of oxidized products containing two chlorine atoms. However, reducing the reaction temperature provided greater control, and we isolated green compound **4d** with one new C–C bond in 30% yield. We also observed a trace amount of double-oxidized **2d**. Extension of the reaction time to 7 d increased the amount of **2d**, which was isolated in 36% yield.

Oxidation of **1e** at 80 °C led only to decomposition of the substrate and formation of a black reaction mixture with no detectable amount of desired products. Reducing the temperature to 0 °C resulted in the selective formation of single oxidized green product **4e** in 32% isolated yield. Attempts to achieve the fully oxidized product were unsuccessful and resulted only in decomposition. Finally, tri(2-pyrenyl)azulene **1f** was subjected to Scholl-type oxidation, resulting in the fully oxidized brown compound **2f** in 46% isolated yield. The presence of K_2CO_3 was also important for pyrene-containing substrates, and without K_2CO_3, we observed mainly decomposition.

Compound **2f** is a double [5]helicene, which may have a significant racemization barrier,[54] leading to the potential formation of different isomers: the *meso* (*P*,*M*) form or a racemic mixture of (*P*,*P*) and (*M*,*M*) stereoisomers. Only one set of signals was observed in the ^{1}H NMR spectrum, suggesting the presence of only one form in solution. Despite numerous attempts, we were unable to obtain crystals of **2f** suitable for X-ray single crystal diffraction. Density functional theory (DFT) calculations indicated that there was 8.72 kJ mol^{-1} lower energy for the *meso* form than the chiral form (ESI, Fig. S16‡), and thus, the *meso* conformer was used for further analysis.

A particularly intriguing question is why different substitution patterns lead to different reactivity patterns. It is known that a 1,2-shift of a phenyl substituent can sometimes occur during Scholl oxidation, resulting in unexpected products.[55,56] However, no examples of such a 1,2-shift involving an azulene precursor have been reported to date. Generally, two mechanisms are considered for Scholl oxidation: the arene cation mechanism and radical cation mechanism. In our case, the reaction occurs under basic conditions, leading us to assume that the radical cation mechanism occurred, where the initial step involves the abstraction of one electron from the substrate. Analysis of the spin density might be employed as a convenient tool to understand the observed reactivity[53] because carbon atoms with positive spin density are expected to be involved in the formation of new C–C bonds. To gain further insights into the reactivity observed during Scholl oxidation, we conducted DFT calculations of possible intermediate radical cations at the UB3LYP/6-31G(d) level of theory.

The spin densities calculated for radical cations directly formed from compounds **1** showed significant difference regarding the substituent in position 2 of azulene (ESI, Fig. S15‡). When a 2-pyrenyl substituent is present in position 2 of azulene $(\mathbf{1d})^{\bullet+}$ and $(\mathbf{1f})^{\bullet+}$, significant spin density is observed on the relevant carbon atoms contrary to the compounds $(\mathbf{1a})^{\bullet+}$ and $(\mathbf{1e})^{\bullet+}$, which should facilitate the desired oxidation of the former. Comparing the DFT-calculated spin densities of radical cations after the formation of the first C–C bond (Fig. 1) highlights notable differences.

The carbon atoms involved in the formation of the second C–C bond are depicted in C1–C3. In the case of radical cations $(\mathbf{4d})^{\bullet+}$ and $(\mathbf{4f})^{\bullet+}$, significant positive spin density was observed at the C1 carbon atom. The spin density at the C2/C3 atoms was smaller in the case of $(\mathbf{4d})^{\bullet+}$ as compared to $(\mathbf{4f})^{\bullet+}$, which explains the easy double oxidation of **1f**. There is no C1 positive spin for $(\mathbf{4a})^{\bullet+}$ and $(\mathbf{4e})^{\bullet+}$, which explains the alternative 1,2-phenyl shift pathway in the case of the first, and decomposition at higher temperature for the latter. Interestingly, a

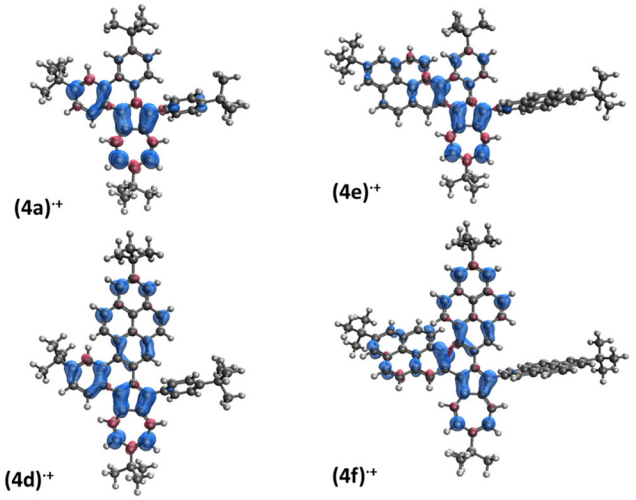

	(4a)$^{\cdot+}$	(4d)$^{\cdot+}$	(4e)$^{\cdot+}$	(4f)$^{\cdot+}$
C1	-0.019	0.158	-0.024	0.083
C2	0.034	0.003	0.024	0.096
C3	0.035	0.005	0.012	0.071

Fig. 1 Spin density distribution of radical cations after formation of the first C–C bond, UB3LYP/6-31G(d).

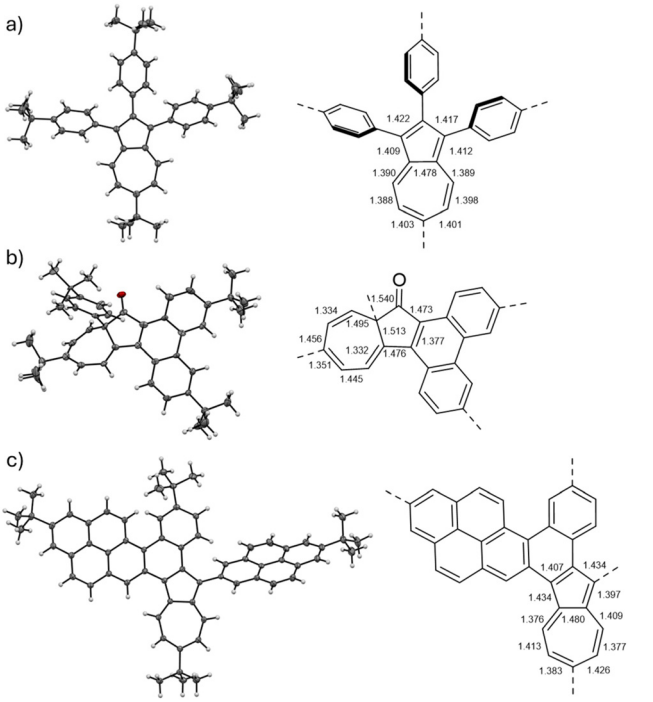

Fig. 2 The molecular structures and selected bond lengths (Å) of (a) compound **1a**; (b) compound **3a**, one of three molecules in the asymmetric unit, where bond lengths are the mean of the bond lengths of the molecules in the asymmetric unit; (c) compound **4e**, with ellipsoids given at 50% probability.

similar distribution of spin density over the pyrene moiety has been shown to play a key role in the selectivity of the Scholl reaction in fully benzenoid substrates.[53]

We acknowledge that fully elucidating the mechanism of the Scholl reaction is a great challenge, and many aspects of such reactions remain debatable in the literature. In our view, the key distinction between fully benzenoid and azulene-containing precursors in the Scholl reaction is the high-lying HOMO of azulene. Consequently, the intermediate radical cation has its positive spin density primarily localized on the azulene moiety, facilitating alternative reaction pathways. This contrast is evident when compared to the reactivity of 1,2,3,4-tetraphenylnaphthalenes, which exclusively yield the typical products of the Scholl reaction under various oxidation conditions.[57–59] Nonetheless, these results bring us closer to understanding the elusive reaction mechanism in azulene-containing substrates and provide insights into predicting the outcomes of Scholl-type oxidations.

X-ray single crystal diffraction

X-ray single crystal experiments were conducted to confirm the molecular structures of the oxidation products. Single crystals of compounds **1a** and **3a** were obtained (Fig. 2a and b), unequivocally confirming the occurrence of a 1,2-phenyl shift, followed by oxidation at position 1 of azulene and the formation of a new C–C bond. Compound **3a** crystallizes with three molecules in the asymmetric unit in the chiral point group $P2_12_12_1$, existing as a 2 : 1 mixture of two enantiomers.

Analysis of the experimental bond lengths reveals a significant change from the initial geometry and electronic structure of the azulene unit compared to substrate **1a**. The bridging carbon atom adopts an sp^3 hybridization, disrupting conjugation and resulting in an alternating pattern of double and single C–C bonds. Disappearance of azulene-like geometry and electronic structure explains the yellow colour observed in compounds **3a–3c**.

Single crystals of compound **4e** suitable for X-ray experiments were obtained by a slow diffusion of MeOH vapours into its solution in *ortho*-dichlorobenzene. X-ray crystallography unambiguously confirmed the identity of **4e** (Fig. 2c). Notably, compound **4e** retained the azulene unit's geometry, suggesting that the azulene-like electronic structure remained present. The carbon–carbon bond lengths of the azulene moiety in **4e** are similar to the geometry of unsubstituted azulene.[60] The entire π-scaffold is slightly warped due to the presence of the [4]helicene moiety.

Electronic and optical properties

The optical properties of all oxidation products were studied in CH_2Cl_2 solution. The absorption of compounds **3a–3c** occurs mainly in the UV region due to the broken conjugation in the former azulene moiety, resulting in a pale yellow colour (ESI, Fig. S1–S3‡). In contrast, the absorption spectra of the fused azulenes **2d**, **4d**, **4e**, and **2f** are far more complex (Fig. 3a). Extended azulenes **4d** and **4e** exhibit the lowest energy transition above 680 nm (Table 2), which, according to the time-dependent (TD)-DFT calculations, corresponds to an almost

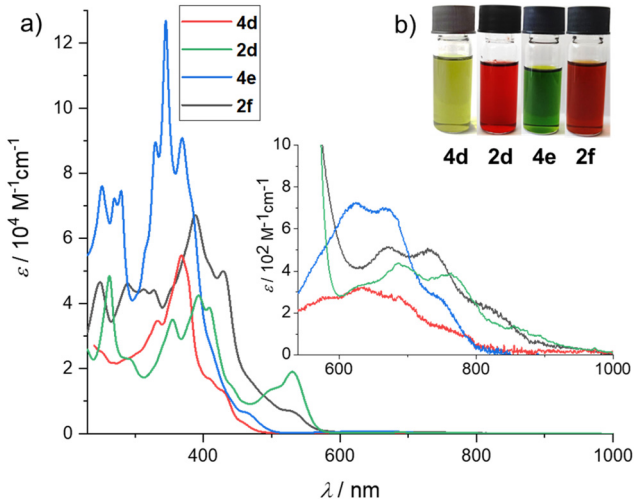

Fig. 3 (a) UV/Vis/NIR spectra of compounds **4d**, **2d**, **4e**, and **2f** (CH_2Cl_2, *c* approximately 10^{-6} M, 20 °C). (b) Photographs of CH_2Cl_2 solutions of **4d**, **2d**, **4e**, and **2f**.

forbidden $S_0 \rightarrow S_1$ transition ($f = 0.024$ for **4d** and $f = 0.037$ for **4e**) primarily involving the HOMO to LUMO transition component (ESI, Tables S5–S8‡). This transition is responsible for the distinctive green colour of **4d** and **4e** (Fig. 3b).

Similar low-energy transitions are present in the spectra of the fully fused azulenes **2d** and **2f**, but these are more red-shifted, reaching up to 764 nm in the case of compound **2d**. This trend is in accordance with the outcome of the TD-DFT calculations (ESI, Tables S5–S8‡). Such a low energy transition is the result of the retained azulene-like electronic structure in fully and partially fused π-scaffolds. The spatial separation of the HOMO and LUMO orbitals resembles those of pristine azulene, as clearly visible in Fig. 4. Therefore, these compounds can be regarded as 'true' extended azulenes, unlike many azulene-embedded PAHs reported in the literature, which are merely benzenoid PAHs with seven- and five-membered rings serving as linkages between adjacent benzenoid moieties.

In the case of fully fused **2d** and **2f**, a distinctive HOMO to LUMO+1 $S_0 \rightarrow S_2$ transition above 500 nm was primarily

Table 2 Selected electrochemical[a] and optical properties of **4d**, **2d**, **4e**, and **2f**

Compound	$E^{ox}_{1/2}$ [V]	$E^{red}_{1/2}$ [V]	ΔE [V]	E_{HOMO} [b] [eV]	E_{LUMO} [b] [eV]	λ_{max} [c] (exp.) [nm]	λ_{max} [c] (exp.) [eV]	λ_{max} [d] (DFT) [nm]	λ_{max} [d] (DFT) [eV]
4d	0.30	−1.92	2.22	−5.10	−2.88	687	1.80	617	2.01
2d	0.10	−1.81	1.91	−4.90	−2.99	764	1.62	692	1.79
4e	0.35	−1.90	2.25	−5.15	−2.90	689	1.80	605	2.05
2f	0.29	−1.60	1.89	−5.09	−3.20	733	1.69	677	1.83

[a] Working/counter electrodes: Pt disc/wire, respectively; reference electrode: Ag/AgCl; scan rate: 50 mV s^{-1}; concentration: approximately 10^{-5} M in CH_2Cl_2 containing 0.1 M $[NBu_4][PF_6]$ as the supporting electrolyte. All redox potentials were calibrated against the Fc/Fc^+ standard. [b] Calculated according to the known procedure using the experimentally determined redox potentials ($E_{LUMO} = -(E_{red} + 4.8\ eV)$ and $E_{HOMO} = -(E_{ox} + 4.8\ eV)$) and the energy level of Fc^+/Fc with respect to the vacuum level (−4.8 eV).[61] [c] Measured for CH_2Cl_2 solutions, *c* approximately 10^{-5} M. [d] Calculated at B3LYP/6-31G(d) level of theory, $S_0 \rightarrow S_1$ transitions.

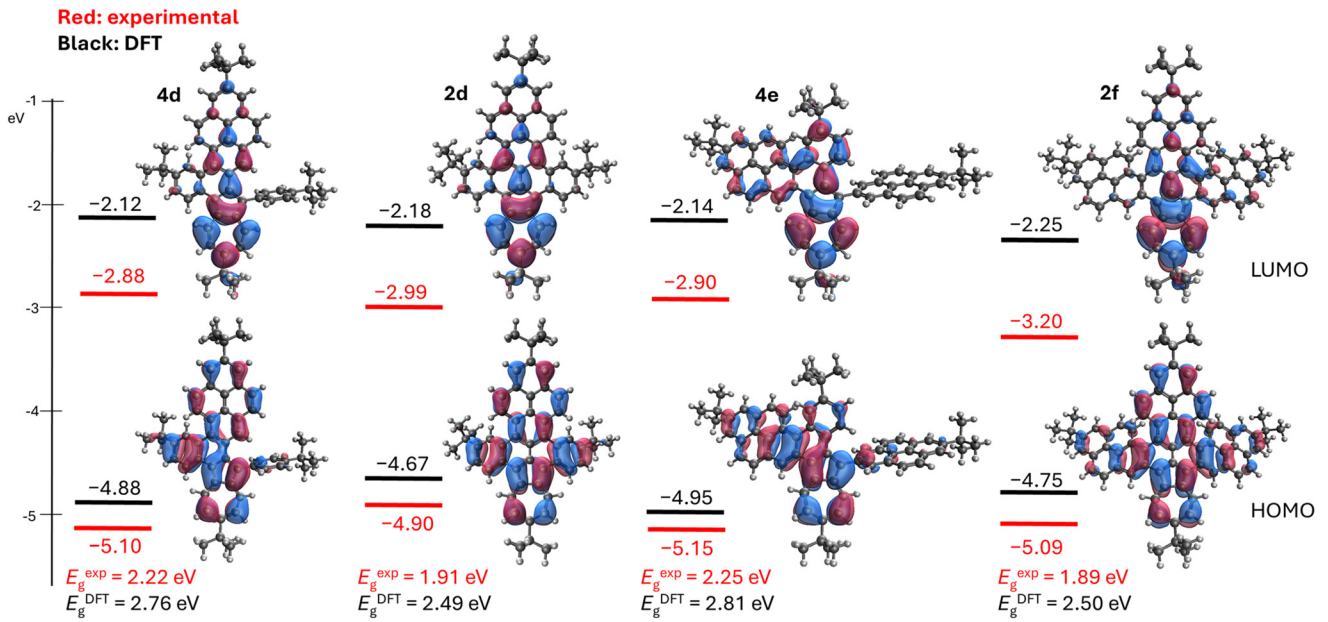

Fig. 4 DFT-calculated (B3LYP/6-31G(d), isovalue 0.05 A^{-3}) and experimental energies of HOMO and LUMO orbitals of **4d**, **2d**, **4e**, and **2f**.

responsible for their red colour, as it is much stronger than the almost forbidden $S_0 \rightarrow S_1$ transition (oscillator strength f = 0.680 for **2d** and f = 0.380 for **2f**). Although some of the known extended azulenes exhibited fluorescence, we did not observe Kasha nor *anti*-Kasha emission for the compounds reported here.

Electrochemical measurements of the reported azulene-embedded PAHs were carried out to experimentally estimate the HOMO and LUMO energy levels. Cyclic voltammetry (CV) and differential pulse voltammetry (DPV) measurements were implemented for all extended azulenes (ESI, Fig. S8–S14‡). All compounds exhibited relatively low, reversible first oxidation potentials, ranging from 0.10 V *vs.* Fc/Fc^+ for **2d** to 0.35 V *vs.* Fc/Fc^+ for **4e**. This corresponds to the relatively high-lying HOMO orbitals (Fig. 4), and is consistent with the highest DFT-calculated HOMO energy for **2d**.

The difference between fully fused π-scaffolds (**2d**, **2f**) and partially fused molecules (**4d**, **4e**) was also evident in their first reduction potentials. Compounds **2d** and **2f** are easier to reduce, with $E^{red}_{1/2}$ = −1.81 V for the former and $E^{red}_{1/2}$ = −1.60 V for the latter compared with $E^{red}_{1/2}$ = −1.90 V for **4e** and $E^{red}_{1/2}$ = −1.92 V for **4d**. The electrochemical gap is smaller for fully fused molecules **2d** and **2f** (approximately 1.9 V), compared to partially fused azulenes, which have an electrochemical gap above 2.2 V. This trend is in alignment with the DFT calculations (Fig. 4) and is due to both the lower energies of the LUMO orbitals and the higher energies of the HOMO orbitals. Notably, the electrochemical and optical gaps of the fully fused-azulenes reported here are significantly narrower than those of benz[*a*]azulenes[28] ($E^{electr}_g \approx 3.0$ eV; $E^{opt}_g \approx 2.6$ eV) or azuleno[1,2,3-*fg*]benzo[*op*]tetracene[38] (E^{electr}_g = 2.18 eV; E^{opt}_g = 1.78 eV).

Finally, we calculated the NICS(0) values[62] of azulene-embedded PAHs **4d**, **2d**, **4e**, and **2f** (ESI, Fig. S24‡). The NICS (0) values confirmed the retained aromatic characteristics of the azulene moiety, which are in agreement with the ^{1}H NMR chemical shifts and all the optical and electrochemical properties. This serves as additional confirmation that the reported PAHs are truly extended azulenes, not simply benzenoid structures with bridging five- and seven-membered rings.

Conclusions

Our investigations revealed that Scholl oxidation of relatively simple 1,2,3-triarylazulenes can result in unexpected reactivity patterns, including a 1,2-shift of a phenyl group and the formation of azulen-1(8a*H*)-ones. However, incorporating 2-pyrenyl substituents facilitated the formation of fused azulene structures, which was likely due to the favourable spin density distribution in the intermediate radical cations. This synthetic route enabled us to obtain a series of 'true' π-extended azulenes with optical absorption reaching the NIR region and a relatively low electrochemical gap below 2 eV. A synthetic strategy involving 2-pyrenyl substituents is promising for the construction of larger, fully hydrocarbon nanographenes incorporating multiple azulene subunits. This approach is currently being further developed in our laboratory.

Author contributions

All authors have given approval to the final version of the manuscript. CRediT: Justyna Biesaga: conceptualization, investigation, writing – review and editing; Sławomir Szafert: supervision; Bartłomiej Pigulski: conceptualization, funding acquisition, investigation, supervision, writing – original draft, writing – review and editing.

Data availability

The data supporting this article have been included as part of the ESI.‡ The crystallographic data for **1a**, **3a**, and **4e** have been deposited at the CCDC under 2371233–2371235.‡

Conflicts of interest

There are no conflicts to declare.

Acknowledgements

The authors thank the National Science Centre Poland (Grant UMO-2022/47/D/ST4/03312) for support of this research. Calculations were carried out at the Wrocław Centre for Networking and Supercomputing (**https://www.wcss.pl**), Grant No. 523.

References

1 A. Hirsch, The era of carbon allotropes, *Nat. Mater.*, 2010, **9**, 868–871.
2 Z. Liu, S. Fu, X. Liu, A. Narita, P. Samorì, M. Bonn and H. I. Wang, Small Size, Big Impact: Recent Progress in Bottom-Up Synthesized Nanographenes for Optoelectronic and Energy Applications, *Adv. Sci.*, 2022, **9**, 2106055.
3 A. Narita, X. Y. Wang, X. Feng and K. Müllen, New advances in nanographene chemistry, *Chem. Soc. Rev.*, 2015, **44**, 6616–6643.
4 A. Konishi and M. Yasuda, Breathing new life into nonalternant hydrocarbon chemistry: Syntheses and properties of polycyclic hydrocarbons containing azulene, pentalene, and heptalene frameworks, *Chem. Lett.*, 2021, **50**, 195–212.
5 Chaolumen, I. A. Stepek, K. E. Yamada, H. Ito and K. Itami, Construction of Heptagon-Containing Molecular Nanocarbons, *Angew. Chem., Int. Ed.*, 2021, **60**, 23508–23532.
6 K. Kawasumi, Q. Zhang, Y. Segawa, L. T. Scott and K. Itami, A grossly warped nanographene and the consequences of

multiple odd-membered-ring defects, *Nat. Chem.*, 2013, **5**, 739–744.

7 M. Beer and H. C. Longuet-Higgins, Anomalous Light Emission of Azulene, *J. Chem. Phys.*, 1955, **23**, 1390–1391.

8 D. Dunlop, L. Ludvíková, A. Banerjee, H. Ottosson and T. Slanina, Excited-State (Anti)Aromaticity Explains Why Azulene Disobeys Kasha's Rule, *J. Am. Chem. Soc.*, 2023, **145**, 21569–21575.

9 A. G. Anderson and B. M. Steckler, Azulene. VIII. Spectra and Dipole Moments of Substituted Azulenes A Study of the Visible Absorption Spectra and Dipole Moments of Some 1- and 1,3-Substituted Azulenes, *J. Am. Chem. Soc.*, 1959, **81**, 4941–4946.

10 C. Zhu, K. Shoyama and F. Würthner, Conformation and Aromaticity Switching in a Curved Non-Alternant sp^2 Carbon Scaffold, *Angew. Chem., Int. Ed.*, 2020, **59**, 21505–21509.

11 J. Liu, S. Mishra, C. A. Pignedoli, D. Passerone, J. I. Urgel, A. Fabrizio, T. G. Lohr, J. Ma, H. Komber, M. Baumgarten, C. Corminboeuf, R. Berger, P. Ruffieux, K. Müllen, R. Fasel and X. Feng, Open-Shell Nonbenzenoid Nanographenes Containing Two Pairs of Pentagonal and Heptagonal Rings, *J. Am. Chem. Soc.*, 2019, **141**, 12011–12020.

12 A. Konishi, K. Horii, D. Shiomi, K. Sato, T. Takui and M. Yasuda, Open-shell and antiaromatic character induced by the highly symmetric geometry of the planar heptalene structure: Synthesis and characterization of a nonalternant isomer of bisanthene, *J. Am. Chem. Soc.*, 2019, **141**, 10165–10170.

13 B. Pigulski, K. Shoyama and F. Würthner, NIR-Absorbing π-Extended Azulene: Non-Alternant Isomer of Terrylene Bisimide, *Angew. Chem., Int. Ed.*, 2020, **59**, 15908–15912.

14 H. Xin, B. Hou and X. Gao, Azulene-Based π-Functional Materials: Design, Synthesis, and Applications, *Acc. Chem. Res.*, 2021, **54**, 1737–1753.

15 H. Xin and X. Gao, Application of Azulene in Constructing Organic Optoelectronic Materials: New Tricks for an Old Dog, *ChemPlusChem*, 2017, **82**, 945–956.

16 H. Xin, C. Ge, X. Yang, H. Gao, X. Yang and X. Gao, Biazulene diimides: A new building block for organic electronic materials, *Chem. Sci.*, 2016, **7**, 6701–6705.

17 E. Puodziukynaite, H. W. Wang, J. Lawrence, A. J. Wise, T. P. Russell, M. D. Barnes and T. Emrick, Azulene methacrylate polymers: Synthesis, electronic properties, and solar cell fabrication, *J. Am. Chem. Soc.*, 2014, **136**, 11043–11049.

18 Y. Yamaguchi, M. Takubo, K. Ogawa, K. I. Nakayama, T. Koganezawa and H. Katagiri, Terazulene Isomers: Polarity Change of OFETs through Molecular Orbital Distribution Contrast, *J. Am. Chem. Soc.*, 2016, **138**, 11335–11343.

19 T. Shoji, K. Miura, T. Araki, A. Maruyama, A. Ohta, R. Sekiguchi, S. Ito and T. Okujima, Synthesis of 2-Methyl-1-azulenyl Tetracyanobutadienes and Dicyanoquinodimethanes: Substituent Effect of 2-Methyl Moiety on the Azulene Ring toward the Optical and Electrochemical Properties, *J. Org. Chem.*, 2018, **83**, 6690–6705.

20 H. Xin, C. Ge, X. Jiao, X. Yang, K. Rundel, C. R. McNeill and X. Gao, Incorporation of 2,6—Connected Azulene Units into the Backbone of Conjugated Polymers: Towards High–Performance Organic Optoelectronic Materials, *Angew. Chem., Int. Ed.*, 2018, **57**, 1322–1326.

21 L. C. Murfin, M. Weber, S. J. Park, W. T. Kim, C. M. Lopez-Alled, C. L. McMullin, F. Pradaux-Caggiano, C. L. Lyall, G. Kociok-Köhn, J. Wenk, S. D. Bull, J. Yoon, H. M. Kim, T. D. James and S. E. Lewis, Azulene-Derived Fluorescent Probe for Bioimaging: Detection of Reactive Oxygen and Nitrogen Species by Two-Photon Microscopy, *J. Am. Chem. Soc.*, 2019, **141**, 19389–19396.

22 S. Cai, W. Deng, F. Huang, L. Chen, C. Tang, W. He, S. Long, R. Li, Z. Tan, J. Liu, J. Shi, Z. Liu, Z. Xiao, D. Zhang and W. Hong, Light–Driven Reversible Intermolecular Proton Transfer at Single–Molecule Junctions, *Angew. Chem., Int. Ed.*, 2019, **58**, 3829–3833.

23 A. Jarszak-Tyl, B. Pigulski and S. Szafert, Solvent-free C-H alkynylation of azulenes, *Org. Chem. Front.*, 2021, **8**, 5674–5680.

24 A. H. M. Elwahy, I. A. Abdelhamid and M. R. Shaaban, Recent Advances in the Functionalization of Azulene Through Pd-Catalyzed Cross-Coupling Reactions, *ChemistrySelect*, 2021, **6**, 13664–13723.

25 A. H. M. Elwahy, M. R. Shaaban and I. A. Abdelhamid, Recent advances in the functionalization of azulene through Rh-, Ir-, Ru-, Au-, Fe-, Ni-, and Cu-catalyzed reactions, *Appl. Organomet. Chem.*, 2022, **36**, e6772.

26 Y. Fei and J. Liu, Synthesis of Defective Nanographenes Containing Joined Pentagons and Heptagons, *Adv. Sci.*, 2022, **9**, 2201000.

27 M. Murai, S. Iba, H. Ota and K. Takai, Azulene-Fused Linear Polycyclic Aromatic Hydrocarbons with Small Bandgap, High Stability, and Reversible Stimuli Responsiveness, *Org. Lett.*, 2017, **19**, 5585–5588.

28 A. Vardanyan, A. Villinger, P. Ehlers and P. Langer, Synthesis and Properties of Carbo- and Heterocyclic Benz [*a*]azulenes, *J. Org. Chem.*, 2023, **88**, 11411–11423.

29 C. Duan, J. Zhang, J. Xiang, X. Yang and X. Gao, Azulene-Embedded [*n*]Helicenes (*n*=5, 6 and 7), *Angew. Chem., Int. Ed.*, 2022, **61**, e202201494.

30 R. Liu, Y. Fu, F. Wu, F. Liu, J. J. Zhang, L. Yang, A. A. Popov, J. Ma and X. Feng, Modular Synthesis of Structurally Diverse Azulene-Embedded Polycyclic Aromatic Hydrocarbons by Knoevenagel-Type Condensation, *Angew. Chem., Int. Ed.*, 2023, **62**, e202219091.

31 Q. Jiang, T. Tao, H. Phan, Y. Han, T. Y. Gopalakrishna, T. S. Herng, G. Li, L. Yuan, J. Ding and C. Chi, Diazuleno–*s*–indacene Diradicaloids: Syntheses, Properties, and Local (anti)Aromaticity Shift from Neutral to Dicationic State, *Angew. Chem., Int. Ed.*, 2018, **57**, 169737–116741.

32 Y. Liang, S. Wang, M. Tang, L. Wu, L. Bian, L. Jiang, Z.-B. Tang, J. Liu, A. Guan and Z. Liu, Cascade Synthesis of Benzotriazulene with Three Embedded Azulene Units and Large Stokes Shifts, *Angew. Chem., Int. Ed.*, 2023, **62**, e202218839.

33 J. Wang, F. G. Gámez, J. Marín-Beloqui, A. Diaz-Andres, X. Miao, D. Casanova, J. Casado and J. Liu, Synthesis of a Dicyclohepta[*a*,*g*]heptalene-Containing Polycyclic Conjugated Hydrocarbon and the Impact of Non-Alternant Topologies, *Angew. Chem., Int. Ed.*, 2023, **62**, e202217124.

34 H. Xin, J. Li, R. Q. Lu, X. Gao and T. M. Swager, Azulene-Pyridine-Fused Heteroaromatics, *J. Am. Chem. Soc.*, 2020, **142**, 13598–13605.

35 M. Grzybowski, K. Skonieczny, H. Butenschön and D. T. Gryko, Comparison of Oxidative Aromatic Coupling and the Scholl Reaction, *Angew. Chem., Int. Ed.*, 2013, **52**, 9900–9930.

36 M. Grzybowski, B. Sadowski, H. Butenschön and D. T. Gryko, Synthetic Applications of Oxidative Aromatic Coupling—From Biphenols to Nanographenes, *Angew. Chem., Int. Ed.*, 2020, **59**, 2998–3027.

37 H. N. Zeng, Z. M. Png and J. Xu, Azulene in Polymers and Their Properties, *Chem. – Asian J.*, 2020, **15**, 1904–1915.

38 Chaolumen, H. Ito and K. Itami, An axially chiral 1,1′-biazulene and its π-extended derivative: Synthesis, structures and properties, *Chem. Commun.*, 2019, **55**, 9606–9609.

39 P. Mathey, I. Fernández and J. F. Morin, Exploring C-C bond formation reactions for expanding azulene derivatives linked at the 2- and/or 6-positions, *New J. Chem.*, 2024, **48**, 4801–4809.

40 T. Koide, M. Takesue, T. Murafuji, K. Satomi, Y. Suzuki, J. Kawamata, K. Terai, M. Suzuki, H. Yamada, Y. Shiota, K. Yoshizawa and F. Tani, An Azulene-Fused Tetracene Diimide with a Small HOMO–LUMO Gap, *ChemPlusChem*, 2017, **82**, 1010–1014.

41 L. Chen, B. Wu, L. Qin, Y. Y. Huang, W. Meng, R. Kong, X. Yu, K. ChenChai, C. Li, G. Zhang, X. S. Zhang and D. Zhang, A perylene five-membered ring diimide for organic semiconductors and π-expanded conjugated molecules, *Chem. Commun.*, 2022, **58**, 5100–5103.

42 D. Eppel, N. Oberhof, M. C. Dietl, P. Cieslik, M. Rudolph, L. Eberle, P. Krämer, F. Stuck, F. Rominger, A. Dreuw and A. S. K. Hashmi, Gold(III) Meets Azulene: A Class of [($^{t\text{Bu}}$C^N^C)Au$^{\text{III}}$(azulenyl)] Pincer Complexes, *Organometallics*, 2021, **40**, 3865–3870.

43 P. de Wit, H. J. A. Lambrechts and H. Cerfontain, On the bromination of 1,2,3-triphenylazulene, *Recl. Trav. Chim. Pays-Bas*, 1985, **104**, 68–69.

44 S. J. Assony and N. Kharasch, Derivatives of Sulfenic Acids. XXXII. The Synthesis of Azulenes *via* the Interactions of Arylacetylenes with Sulfenyl Halides. Part 1. 1,2,3-Triphenylazulene, *J. Am. Chem. Soc.*, 1958, **80**, 5978–5982.

45 C. Lambert, G. Nöll, M. Zabel, F. Hampel, E. Schmälzlin, C. Bräuchle and K. Meerholz, Highly substituted azulene dyes as multifunctional NLO and electron-transfer compounds, *Chem. – Eur. J.*, 2003, **9**, 4232–4239.

46 V. Claus, M. Schukin, S. Harrer, M. Rudolph, F. Rominger, A. M. Asiri, J. Xie and A. S. K. Hashmi, Gold-Catalyzed Dimerization of Diarylalkynes: Direct Access to Azulenes, *Angew. Chem., Int. Ed.*, 2018, **57**, 12966–12970.

47 T. D. Lash, J. A. El-Beck and G. M. Ferrence, Syntheses and reactivity of meso-unsubstituted azuliporphyrins derived from 6-*tert*-butyl- and 6-phenylazulene, *J. Org. Chem.*, 2007, **72**, 8402–8415.

48 M. Narita, T. Murafuji, S. Yamashita, M. Fujinaga, K. Hiyama, Y. Oka, F. Tani, S. Kamijo and K. Ishiguro, Synthesis of 2-Iodoazulenes by the Iododeboronation of Azulen-2-ylboronic Acid Pinacol Esters with Copper(I) Iodide, *J. Org. Chem.*, 2018, **83**, 1298–1303.

49 K. H. Chen, Y. J. Chiang and J. L. Zhu, Rhodium-catalyzed cyclization of acceptor-substituted biphenyl α-diazoketones: A study of the substitution effect on chemoselectivity, *Org. Biomol. Chem.*, 2018, **16**, 6975–6986.

50 S. A. More, V. A. Sadaphal, T. C. Kuo, M. J. Cheng and R. S. Liu, Reactions of thioalkynes with diarylketenes *via* [3+2]-annulation *versus* benzannulation using Au and $P(C_6F_5)_3$ catalysts, *Chem. Commun.*, 2022, **58**, 10064–10067.

51 D. G. Brown, T. R. Hoye and R. G. Brisbois, Synthesis of Azulenone Skeletons by Reaction of 2-Phenyl-2-acylketenes [RCO(Ph)C=C=O] with Alkynyl Ethers: Mechanistic Aspects and Further Transformations, *J. Org. Chem.*, 1998, **63**, 1630–1636.

52 X. D. Yue, L. Chen and W. D. Z. Li, Synthesis and applications of angular acyl-substituted azulenones: Formal synthesis of (±)-acorenol and facile access to the hydroazulene core of pseudolaric acid, *Tetrahedron*, 2014, **70**, 5505–5512.

53 S. H. Pun, E. C. H. Wen, Z. Xia, H. Chen, F. R. Fischer and Q. Miao, Reactivity, Regioselectivity, and Synthetic Application of 2-Pyrenyl Units in Scholl Reactions, *CCS Chem.*, 2023, **5**, 2069–2077.

54 P. Ravat, Carbo[*n*]helicenes Restricted to Enantiomerize: An Insight into the Design Process of Configurationally Stable Functional Chiral PAHs, *Chem. – Eur. J.*, 2021, **27**, 3957–3967.

55 M. Krzeszewski, K. Sahara, Y. M. Poronik, T. Kubo and D. T. Gryko, Unforeseen 1,2-Aryl Shift in Tetraarylpyrrolo [3,2-*b*] pyrroles Triggered by Oxidative Aromatic Coupling, *Org. Lett.*, 2018, **20**, 1517–1520.

56 J. Liu, A. Narita, S. Osella, W. Zhang, D. Schollmeyer, D. Beljonne, X. Feng and K. Müllen, Unexpected Scholl Reaction of 6,7,13,14-Tetraarylbenzo[*k*]tetraphene: Selective Formation of Five-Membered Rings in Polycyclic Aromatic Hydrocarbons, *J. Am. Chem. Soc.*, 2016, **138**, 2602–2608.

57 W. Kong, L. H. Finger, J. C. A. Oliveira and L. Ackermann, Rhodaelectrocatalysis for Annulative C–H Activation: Polycyclic Aromatic Hydrocarbons through Versatile Double Electrocatalysis, *Angew. Chem., Int. Ed.*, 2019, **58**, 6342–6346.

58 Z. Guo, J. Zhang, J. Zhang and M. Xie, Electrochemical Rhodium-Catalyzed C-H Cyclodimerization of Alkynes to Access Diverse Functionalized Naphthalenes: Involvement of $Rh^{IV/V}$ and Rh^{I} Dual Catalysis, *Org. Lett.*, 2022, **24**, 7784–7789.

59 Y. Honjo, Y. Shibata, E. Kudo, T. Namba, K. Masutomi and K. Tanaka, Room Temperature Decarboxylative and Oxidative [2+2+2] Annulation of Benzoic Acids with Alkynes

Catalyzed by an Electron-Deficient Rhodium(III) Complex, *Chem. – Eur. J.*, 2018, **24**, 317–321.

60 B. Dittrich, F. P. A. Fabbiani, J. Henn, M. U. Schmidt, P. Macchi, K. Meindl and M. A. Spackman, Azulene revisited: solid-state structure, invariom modeling and lattice-energy minimization of a classical example of disorder, *Acta Crystallogr., Sect. B: Struct. Sci., Cryst. Eng. Mater.*, 2018, **74**, 416–426.

61 I. Seguy, P. Jolinat, P. Destruel, R. Mamy, H. Allouchi, C. Courseille, M. Cotrait and H. Bock, Crystal and Electronic Structure of a Fluorescent Columnar Liquid Crystalline Electron Transport Material, *ChemPhysChem*, 2001, **2**, 448–452.

62 Z. Chen, C. S. Wannere, C. Corminboeuf, R. Puchta, P. Von and R. Schleyer, Nucleus-Independent Chemical Shifts (NICS) as an Aromaticity Criterion, *Chem. Rev.*, 2005, **105**, 3842–3888.